Article

aTrunk—An ALS-Based Trunk Detection Algorithm

Sebastian Lamprecht *, Johannes Stoffels, Sandra Dotzler, Erik Haß, Thomas Udelhoven

Remote Sensing & Geoinformatics Department, Trier University, Behringstraße, Trier 54286, Germany; E-Mails: stoffels@uni-trier.de (J.S.); dotzler@uni-trier.de (S.D.); hass@uni-trier.de (E.H.); udelhoven@uni-trier.de (T.U.)

* Author to whom correspondence should be addressed; E-Mail: lamprecht@uni-trier.de; Tel.: +49-651-2014612.

Abstract: This paper presents a rapid multi-return ALS-based (Airborne Laser Scanning) tree trunk detection approach. The multi-core *Divide & Conquer* algorithm uses a CBH (Crown Base Height) estimation and 3D-clustering approach to isolate points associated with single trunks. For each trunk, a principal-component-based linear model is fitted, while a deterministic modification of *LO-RANSAC* is used to identify an optimal model. The algorithm returns a vector-based model for each identified trunk while parameters like the ground position, zenith orientation, azimuth orientation and length of the trunk are provided. The algorithm performed well for a study area of 109 trees (about $2/3$ Norway Spruce and $1/3$ European Beech), with a point density of 7.6 points per m^2, while a detection rate of about 75% and an overall accuracy of 84% were reached. Compared to crown-based tree detection methods, the *aTrunk* approach has the advantages of a high reliability (5% commission error) and its high tree positioning accuracy (0.59 m average difference and 0.78 m RMSE). The usage of overlapping segments with parametrizable size allows a seamless detection of the tree trunks.

Keywords: airborne LiDAR; stem detection; tree recognition; trunk orientation; clustering; forest; 3D

1. Introduction

1.1. Relevance

For a quantification of environmentally sustainable forest management an exact knowledge of various parameters is needed, e.g., the available number and distribution of trees as well as their species, the timber volume or the LAI (Leaf Area Index) [1]. Remote sensing based single tree characterisation procedures have been proven suitable to enhance forest inventories regarding, for example, ecology, wildlife or biodiversity (e.g., [2,3]). Moreover, growth simulations require single tree models (with features such as height, crown size, tree species, spatial distribution) as input variables [4]. In addition, single tree models have the potential to characterise features of biodiversity (for example, the identification of habitat trees [5]), the tree species [6–8] or the spatial distribution of trees.

1.2. State of the Art

Various approaches have been developed focusing on single tree detection using remote sensing data, while initially spectroscopy images and today mostly ALS (Airborne Laser Scanning) have been used as input data [9]. ALS data has been proven suitable to characterise forest stands on a single tree level ([9–11]). An airborne laser scanner is an active remote sensing system, which provides 3D (three-dimensional) information. Full-waveform and discrete-return ALS systems are distinguished, which are processed in the form of point clouds with additional intensity information [12,13]. Single tree detection relies on pattern recognition methods, which take advantage of the tree phenotype and, if ALS is used, optionally the neighbourhood data of the laser returns [3]. Jakubowski *et al.* [9] mention a general trend towards the usage of ALS alone and a more complex analysis with an increased accuracy of results. For a 2D (two-dimensional) identification and delineation, image-based approaches have been developed, for example watershed or valley-following segmentation techniques [14,15], the *marked point process* technique [16] or object-based image analysis [9]. An adequate identification of suppressed trees relies on the analysis of full-waveform or laser-point data ([11,12,17]). A 3D delineation is possible using voxel-based or vector-based approaches, for example multi-layer imaging techniques [18], variants of *k-means* clustering [19–21], adaptive 3D clustering [22], multi-scale clustering [23] or graph-based methods [2,12]. Generally the 3D approaches result in improved detection rates in vertically inhomogeneous forest stands and more complex and realistic crown shapes [9] compared to raster-based approaches.

1.3. Related Work

The mentioned 3D tree delineation methods are focusing on a crown segmentation which mostly relies on a detection of tree tops based on local maxima (*cf.* [24]). Alternative tree identification approaches focusing on a tree trunk detection are rare.

Reitberger *et al.* [12] present a single tree detection approach, which includes an identification and modelling of tree trunks (ALS point density of 10–25 points per m^2). This method distinguishes trees using a *normalized cut segmentation*, which is capable of using already known tree positions to increase

the accuracy. The initial tree positions are derived by a watershed segmentation method related to Vincent and Soille [25]. Within the segments the CBH (Crown Base Height) is estimated by analysing the vertical histogram. The trunk points are separated within a segment between the CBH and a ground cover threshold. The trunks are identified by a 2D hierarchical clustering, and subsequently modelled by a *RANSAC*-based (*cf.* [26]) line fitting. Reitberger *et al.* [12] defines several rules to the trunk models—minimum number of tree points, minimum length, maximum angle—which shall keep the commission errors low.

The method of Abd Rahman *et al.* [27] uses high density ALS data (70 points per m^2) to identify single trees and model their trunks. Crown segments are identified using a watershed segmentation approach, while the vertical histogram of the points within a segment is evaluated to estimate the crown base height (reference height). The trunk of a segment is identified using a three-dimensional top-down trunk-growing algorithm. The 3D distance, the vertical histogram as well as the trunk diameter are evaluated to decide which points are assigned to the trunk.

The method of Lu *et al.* [28] takes advantage of the ALS intensity values to isolate points associated with trunks from leaf-off deciduous trees (10 points per m^2). The extracted points are used for a three-dimensional bottom-up trunk-growing process, while the assignment is controlled by the least 3D distance and a horizontal distance threshold. To avoid false positives, the trunk length and the maximum height of the lowest trunk point are controlled by threshold values. Furthermore the identified trunks are used for a 3D crown delineation.

Crown-based tree detection approaches usually reach an RMSE in positioning of $0.7\,\text{m}$ up to above $3\,\text{m}$ [11,24,29], which relies—besides the detection technique—on the tree height class (*cf.* [11]). In combination with the derived trunk positions Reitberger *et al.* [12] notices an increased accuracy in positioning by up to $25\,\%$.

1.4. Objective

The *aTrunk* approach shall focus on a rapid ALS-based trunk detection without a dependency on a previous crown identification and shall work seamlessly on the entire observation area. The results shall be suitable to support large scale operational forest surveys, which makes a limited computation effort and data reduction crucial (caused by cost limitations [3]). The unique linear representation of a trunk promises a high reliability of the models, while potentially suppressed trees or dead trunks could be detected too. Applications of the approach could be to use the models as initial positions for crown segmentation approaches (e.g., [12,16]) or to confirm alternatively derived tree positions. An analysis of the trunk characteristics, regarding trunk length, trunk orientation (zenith, azimuth), point distribution in growth direction or spatial tree distribution could give additional information for characterising forest stands and biodiversity.

2. Materials and Methods

2.1. Study Area

The study area—illustrated in Figure 1—is located near the city of Hermeskeil in Rhineland-Palatinate, Germany, at the coordinates $49°48'49''$N, $7°10'3''$E, with an expanse of about $100\,\mathrm{m} \times 80\,\mathrm{m}$ and an area of about $0.5\,\mathrm{ha}$. The examined open forest compartment with tree heights of up to $35\,\mathrm{m}$ was dominated by Norway Spruce (59 trees recorded), but edged by European Beech (16 trees) at the western part of the study area. A measurement campaign on Tuesday, 19 August 2014 derived different types of validation data. This study site was selected, because the forest compartment was to be cleared by a harvester. With this information an analysis of the wood volume can be performed in a further study.
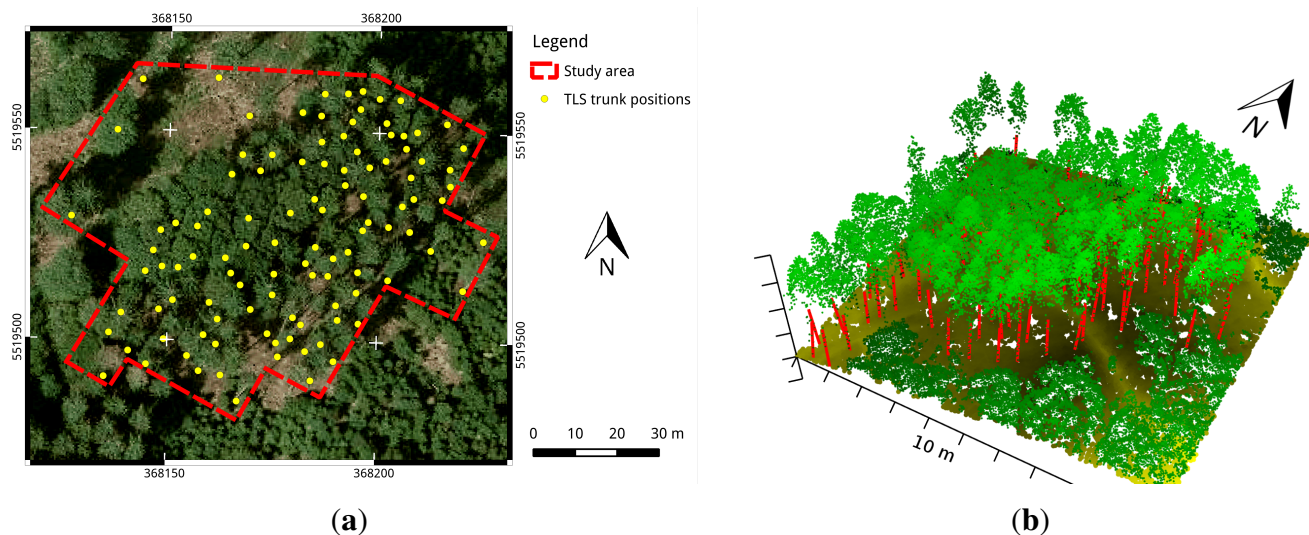

Figure 1. Study area. (**a**) Study area near city of Hermeskeil, Germany with trunk positions predicted by a TLS-based (Terrestrial Laser Scan) trunk detection approach and background WMS-Service [30]. Coordinates are specified in the EPSG:25832 system; (**b**) 3D ALS view of the study area. Yellow-coloured points correspond to ground and green points to vegetation. The brightness values correspond to the elevation. Red lines mark the finally modelled trunks.

2.2. ALS Data

The multi-return ALS data used in this study was collected by the state forest service of Rhineland-Palatinate for the whole federal state, which specifies an absolute horizontal accuracy of $0.30\,\mathrm{m}$ and a vertical accuracy for open terrains of $0.15\,\mathrm{m}$ while a point density of at least 4 points per m^2 is guaranteed. The data was available in form of *ASCII*-files with a spatial expanse of $1\,\mathrm{km} \times 1\,\mathrm{km}$ for each dataset. For the evaluation of the *aTrunk* approach, a subset of the study area of about $125\,\mathrm{m} \times 116\,\mathrm{m}$ (with a extent of [368,112.5, 5,519,462.5, 368,237.5, 5,519,578.0] in EPSG:25832 system) and an overall point density of about 7.6 points per m^2 was chosen. Figure 1b illustrates the

3D structure of the study area. In addition, a full $1\,km^2$ dataset with the extent [368,000, 5,519,000, 369,000, 5,520,000] and an average point density of 7.7 points per m^2 was analysed.

2.3. Validation Data

The validation data collection aimed especially at the position of the trunks because this information can be easily used to estimate the detection rate of the algorithm and the accuracy in modelling the trunk positions. Moreover, ground measurements of the diameter at breast height (DBH) were taken for each trunk, which resulted in an average DBH of $0.255\,m$ with a standard deviation of $0.049\,m$.

For a measurement of the trunk positions, a differential GNSS (Global Navigation Satellite System) of the type *Topcon HiPer V* (*cf.* Topcon Corporation [31]) was used. Because of a poor signal quality, the total accuracies of the measurements were quite low, with location differences clearly above $0.5\,m$.

To gain accurate information about the topology of the trunks, eight terrestrial laser scans (TLS) were taken with a *Laser Scanner Photon 120* of the manufacturer FARO®, which measures at a wavelength of $758\,nm$ and reaches a ranging accuracy of $\pm2\,mm$ at a distance of $25\,m$ (*cf.* FARO Europe GmbH [32]). Each of the all-around scans had a scan size of 8044 × 3446 pixels with the scanner-specific parameters: $1/5$ resolution and $3\times$ quality. The positions of the scans were chosen in such a manner that the study area was mapped completely. The alignment of the single scans to each other was prepared by placing reference spheres which can be identified in the post-processing software.

These TLS datasets were used to estimate the trunk position and diameter by applying a slicing approach (similar to [33]). The slices were $0.05\,m$ thick, beginning at a level of $1.3\,m$ up to the crowning height with a vertical distance of $1\,m$. To compare these models to the *aTrunk* positions, the positions at ground level were estimated by fitting a linear model to the slice centres of each trunk.

2.4. Methods

2.4.1. Preprocessing

The *aTrunk* approach relies on a height-normalised ALS point cloud using a digital terrain model. The delivered ALS data of the study area had already been classified into ground points and non-ground points by the provider. A *Delaunay*-triangulation of the ground points was used to calculate the height above ground for the non-ground points using *CloudCompare* [34].

2.4.2. Assumptions on Trunk Representation

ALS point clouds of different forested areas were visually inspected to define rules for a knowledge-based trunk modelling. The 3D view of the vegetation layer (green highlighted dots in Figure 1b) shows the complex crown structure and allows to identify single trunks because of a linear structure of the corresponding points. The following characteristics of a trunk mapped by ALS are suggested, which form the basis of the trunk model concept outlined in Sections 2.5.3 and 2.5.4:

The LiDAR points associated with a trunk are:

- widely spatially separable from the crown portion and the ground covering vegetation.

- moderately surrounded by points associated with branches, foliage or other objects.
- arranged in a straight line, which is oriented along the growth direction of the trunk. The maximum deviation from this line depends on the length of the trunk, for example, caused by irregular growth or branching.
- largely uniformly distributed in growth direction of the trunk, which is substantiated in the spatial resolution of the ALS data.

2.5. Trunk Detection Algorithm

Figure 2 illustrates the major steps of the presented *aTrunk* approach. The current implementation was realised in *Python* [35]. As base data, the algorithm uses a height-normalised ALS point cloud in the *ASCII*-format.
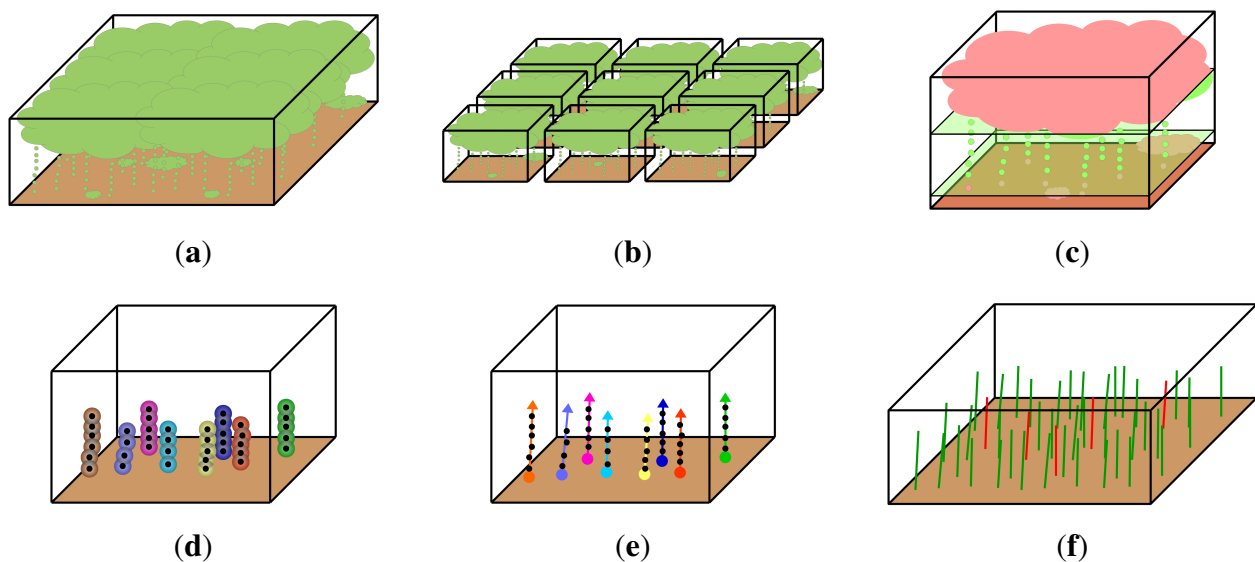

Figure 2. Major steps of the *aTrunk* approach. (**a**) Organisation of the height-normalised points (green) above ground (brown) as a sample S; (**b**) *Divide & Conquer* of the samples to get multiple subsamples; (**c**) Separation of the trunk section for each sample, by using two hyperplanes; (**d**) Trunk identification using a pairwise-distance-based clustering approach; (**e**) Fitting of a 3D principal-component-based linear model to each cluster; (**f**) Merging of the samples, elimination of duplicated trunk models (red lines) and data storage.

2.5.1. Divide & Conquer

The large amount of points makes a direct analysis of the point cloud almost unmanageable. For this reason the idea of introducing a splitting step is used to divide the point cloud into subsets that are easier to handle, which is sketched in Figure 2b. In addition, this procedure facilitates a local estimation of the CBH, which allows a separation of points associated with trunks from other points (see Section 2.5.2).

The input point cloud is stored as an object called sample S, which allows a splitting into two subsamples, while a split is always done in an xy-direction. The size of a sample needs to be selected in such a way that it is small enough to estimate the CBH accurately, but large enough to include at least

one tree. Each sample is separated into two new samples until the extent of the sample falls below a predefined threshold ($maxSampleSize$). This successive splitting allows a multi-core implementation of the algorithm in which it is possible to add a new CPU core to the program after each split.

Nevertheless, the splitting of the point cloud results in some disadvantages, which have to be dealt with. It is possible that points associated with a single trunk are separated from each other at random. This would result in an omission of trees. Therefore an overlapping area along the cutting edge of width $overlap$ is suggested. The implementation of an overlap inevitably results in an additional analysis effort and the possibility of a multiple detection of a single trunk. These repeatedly detected trunks are merged, as described in Section 2.5.5.

2.5.2. Separation of the Trunk Section

The separation of the trunk section is based on the assumption that the potential trunk points P_{TS} lie between points which are associated with ground-covering vegetation and tree crowns (illustrated in Figures 2c and 3b). A first threshold plane at the user-specified height Z_{GCV} detaches the low-growing vegetation. For a sample with a maximum elevation z_{max} it is assumed that the crown base height Z_{CBH} is located in the range $R_{CBH} := [\rho_{min} \cdot z_{max}, \rho_{max} \cdot z_{max}]$. The parameters ρ_{min} and ρ_{max} correspond to the assumed minimum and maximum relative CBH $\rho_{CBH} := \frac{Z_{CBH}}{z_{max}}$ occurring in the study area.
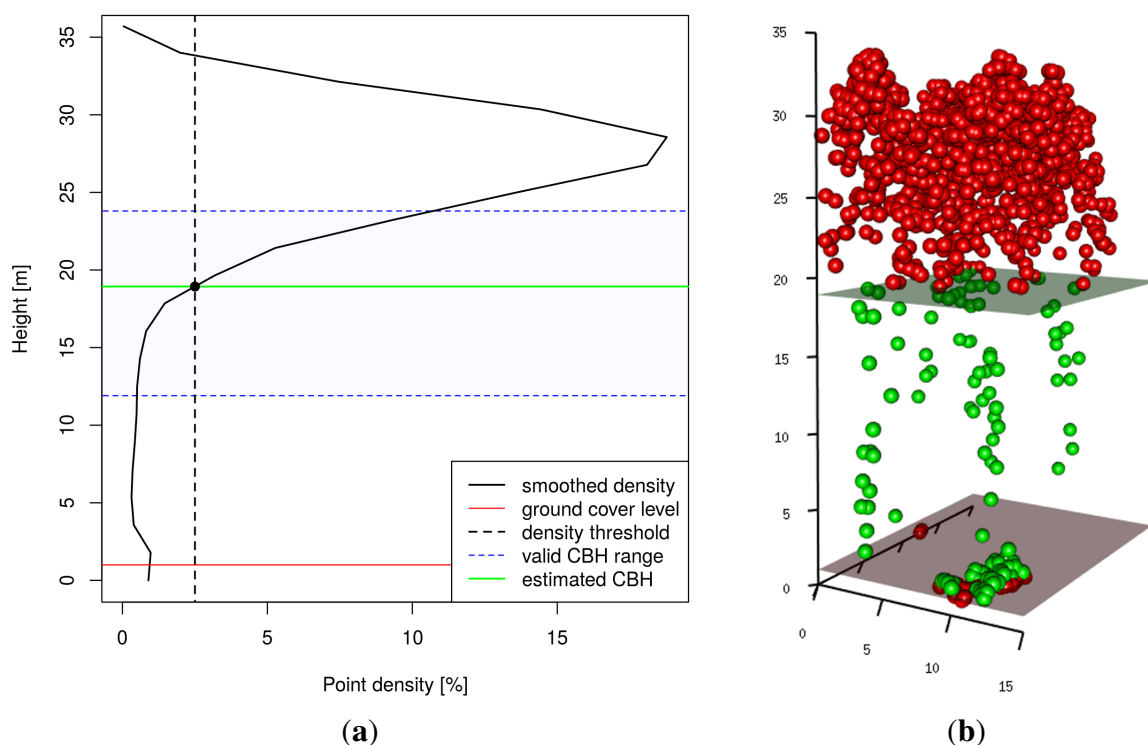

Figure 3. Crown Base Height (CBH) estimation and trunk section separation within a sample. (**a**) The CBH is estimated by identifying the intersection point between the smoothed vertical histogram and a threshold line. Here $N_{layers} = 20$ horizontal layers were used; (**b**) Separation of potential trunk points (green dots) from crown points or low-growing vegetation (red dots).

The CBH is estimated for each sample by analysing the vertical histogram (similarly to [12]). To become independent from the tree height, the points are divided into N_{layers} horizontal layers between Z_{GCV} and z_{max}. The histogram is normalised by dividing the number of points of each layer by the total number of points, and filtered by applying a moving average filter of width 3 (Figure 3a). The estimated CBH corresponds to the highest intersection point where the histogram exceeds the threshold value th. To reduce the dependency of th from the number of layers, it is defined by $th := \frac{thCBH}{N_{layers}}$, while the parameter $thCBH$ is set by the user. If the estimated CBH is located outside the range R_{CBH}—for example caused by a vertically uniform distribution of the points which occurs sometimes for dead trees—it is guessed by $\rho_d \cdot z_{max}$, while the proportion ρ_d is estimated by the user for the study area.

2.5.3. Clustering

The clustering step is used to identify points associated with trunks in the point set P_{TS}. It is assumed that several points which are spatially close together will form a trunk. Isolated points without or with just a few neighbours are assumed to be noise or sparse vegetation. The major problem is to identify point groups without knowing the number of clusters a priori (in contrast to, for example, a *k-Means*-based clustering approach). The proposed cluster definition—as a multi-dimensional extension of the *DBSCAN* [36] approach—takes advantage of the pair-wise spatial neighbourhood of points and the point density to solve this problem.

Cluster Definition: A cluster $C_{p_0,\delta,cMinPts} \subseteq P$ of a point cloud $P \subseteq \mathbb{R}^N$ with dimension N is developed around the initialisation point p_0 using the threshold distance $\delta \in \mathbb{R}^+$ (see Equation (1)). To limit the influence of outliers, each point of the cluster has to have at least $cMinPts$ neighbours with distance δ.

$$C_{p_0,\delta,cMinPts} := \{\, p \in P : |\{\, p_c \in C_{p_0,\delta,cMinPts} \cup \{\, p_0 \,\} : ||p - p_c||_2 \le \delta \,\}| \ge cMinPts \,\} \quad (1)$$

For the purpose of this paper, this cluster definition allows to identify points associated with a single trunk P_{Ct} out of P_{TS} with $N = 3$ (illustrated in Figure 2d). Due to the high vertical variability of the ALS points, the z-coordinates are scaled by the parameter $zBufferScale$ (similar to [23]).

2.5.4. Trunk Model

To get the desired orientation information of the trunks, a linear model is fitted to the points associated with the trunk P_{Ct}. To receive a 3D vector-based regression model, a principal component analysis (PCA) is used.

Basic PCA-Model: A PCA of a point cloud $P \subseteq \mathbb{R}^N$ with $N \in \mathbb{N}$ dimensions provides N pair-wise orthogonal vectors $\overrightarrow{PC_i}$ (with $i \in 1 \ldots N$) which are called principal component (PC) vectors. The PCs define a projected coordinate system, in which the PC scores ($\text{scores}(P) \subseteq \mathbb{R}^N$) of the points P correspond to the projected coordinates of these points in the new coordinate system (*cf.* Wold *et al.* [37]).

The first principal component $t_{\overrightarrow{PC_1}}$ of the point cloud P_{Ct} is oriented in the direction of the highest variance. For a nearly perfect linear alignment of the points associated with the trunk, the $t_{\overrightarrow{PC_1}}$ vector should be oriented in the direction of the trunk. As a data preprocessing, a mean centring of the P_{Ct} points is applied. So the trunk model corresponds to the $t_{\overrightarrow{PC_1}}$ vector which is translated to the original

centre point of the defining P_{Ct} points. The model residuals correspond to the PC scores of the second and third principal component, so these are calculated by Equation (2) (*cf*. p. 9985). Figure 4 illustrates the expected principal component model for a trunk.
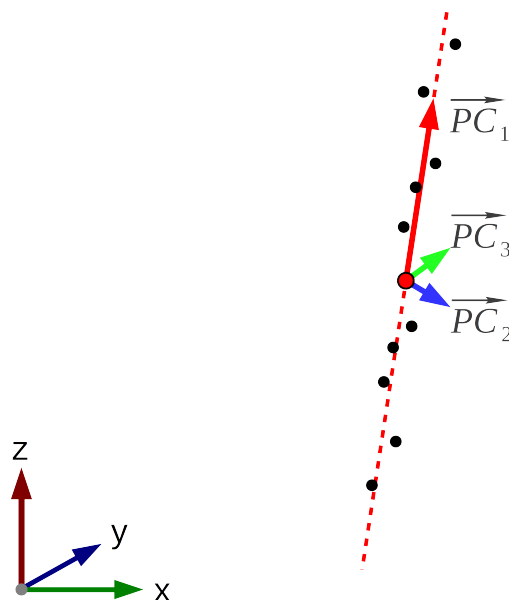

Figure 4. Three-dimensional one component PC trunk modelling concept with P_{Ct} points (black dots) and centre point (red dot).

Unfortunately, the assumption of perfectly linearly arranged points with no kind of outliers cannot be maintained. Therefore an attempt was made to find one PC model which fits most of the points by excluding outliers.

Idea of Best Model Selection: One way to solve the problem of fitting a regression model to highly outlier-affected data is the *RANSAC* approach by Fischler and Bolles [26], which was also used by Reitberger *et al.* [12]. The *RANSAC* approach is based on the assumption that outlying points can be identified by fitting multiple models which each rely on the minimum number of necessary points.

A basic assumption is that the points are randomly chosen and all models are independent from each other. In the case of a PC model, exactly two points are needed for each *RANSAC* sample. After this initialisation, all those points which have a residuum to the model below a specific threshold are assumed to support the model, while the others are assumed to be outliers. The model with the smallest proportion of outliers is accepted as the best model.

In this study the idea of the *LO-RANSAC* approach [38] was used, which optimises the outlier identification by running an additional model fitting for each *RANSAC* sample, using the model-supporting points. This technique relies on $k \approx \frac{\log(\eta)}{\log(1-\epsilon^m)}$ (*cf*. Chum *et al.* [38], p. 2 & 3) random samples to find—with a probability of $P(O)$ % a maximum proportion of O % outliers, with $\epsilon := P(O) \div 100 + 1$ and $\eta := O \div 100 + 1$—a set of at least m inliers. This equation clarifies that the number of points associated with a trunk is insufficient in order to find enough independent points for the common *LO-RANSAC* approach. This is caused by the low number of points associated with a trunk (usually clearly below twenty) and an extremely high proportion of outliers (often caused by ramifications in the upper trunk section or by low-growing vegetation). To derive a deterministic

model, every point pair combination of P_{TS} is defined as an initial pair, whether or not the models are independent.

Model Quality: The quality analysis of a trunk model is divided into two steps. In a first step, the validity of the model is tested, where already one fail results in rejecting the model. In a second step, the model with most model-supporting points is assumed to be the optimum. In case of the same point number, the model with the smallest mean squared error (MSE) is selected. For the validity check, some properties of each model are evaluated according to the modelling parameters summarised in Table 1 (see p. 9988).

A model is assumed to be valid if ...

- it contains enough points to ensure an accurate adaptation but unlikely false detections.
  $\Rightarrow |t_P| \geq n_{min}$
- it contains only some points, because it is assumed that a high number of neighboured points is probably caused by leaves or branches. The value ρ corresponds to the point density of the sample.
  $\Rightarrow |t_P| \leq f_{max} \cdot \rho$
- the range of z is large enough to contain a trunk.
  $\Rightarrow \mathrm{range}\,(t_{P_z}) \geq minZRange$
- the ratio between the z-range (height) and xy-range (width) is comprehensible.
  $\Rightarrow \frac{\mathrm{range}(t_{P_z})}{\max\left(\mathrm{range}(t_{P_x}),\mathrm{range}(t_{P_y})\right)} \geq hwRel$
- the zenith angle of the trunk is reasonable.
  $\Rightarrow t_\zeta \leq maxZenith \in [0, 90[$
- the model has a favourable ratio between model-supporting points and outliers.
  $\Rightarrow \frac{|t_P|+|t_O|}{|t_O|} \leq relOutliers \in [0, 1[$
- the points associated with the trunk are largely uniformly distributed in $t_{\overrightarrow{PC_1}}$ direction.
  $\Rightarrow t_{\chi^2} < uniformProb \in [0, 1]$

Due to the assumption of residuals increasing with the length of the trunk, an adaptable threshold is needed to identify outliers. Therefore a length-dependent quality criterion—called $MEPL$ (Maximum Error Per Length)—is proposed, which shall privilege large trunks in residual weighting. Equation (9) (p. 9987) illustrates the calculation of this criterion, while the still unknown length of the trunk is approximated by the z-values of the points.

Figure 5 illustrates the modified *LO-RANSAC* concept for the PC-based trunk modelling approach, while Figure 2e sketches the modelling results within a sample.

2.5.5. Merge Duplicated Trunks

The split of the samples—done in step 2.5.1—with an intended overlap area can result in a multiple detection of single trunks in the overlapping separation section. This undesired effect is compensated for by an identification and subsequent merging of duplicated trunks whose centres are close together. As it cannot be ruled out that the models differ from each other (caused by a different point basis), all raw points are joined, while duplicates are eliminated. After the merging, a new trunk model is fitted

just as explained in Section 2.5.4. All the derived trunk models are combined again in a result dataset as sketched in Figure 2f.
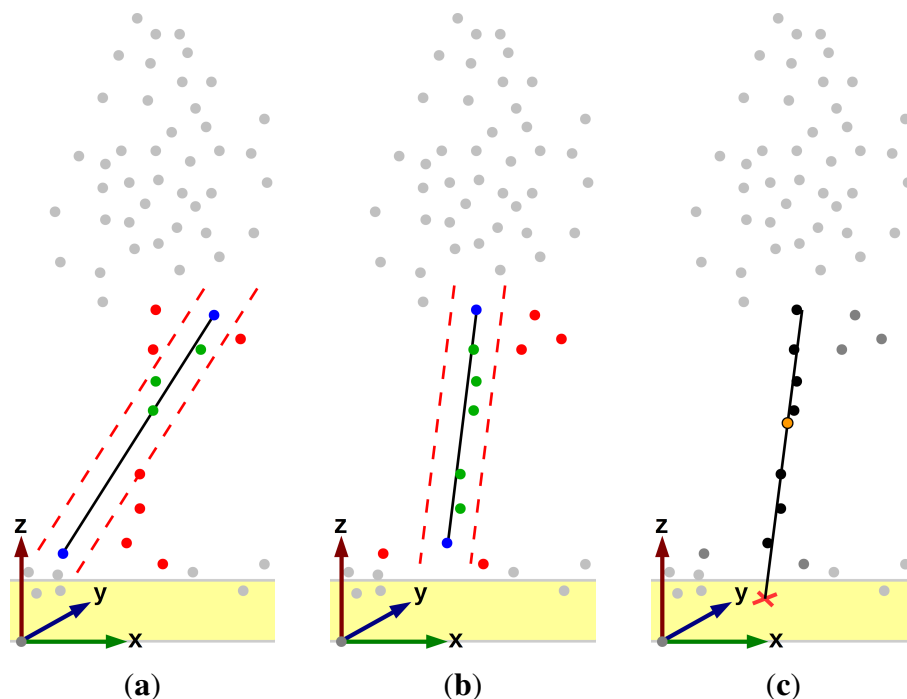

Figure 5. LO-RANSAC-based line fitting approach. Two possible raw trunk models (Figure 5a,b) using two randomly chosen points (blue dots), inlier threshold (red dashed lines), identified inliers (green dots) and outliers (red dots). Grey dots correspond to excluded points. Final model (Figure 5c) using inlier points t_P (black dots), centre point t_c (orange dot) and trunk position t_p (red cross). (**a**) Low quality model in terms of RANSAC; (**b**) High quality model in terms of RANSAC; (**c**) Final trunk model.

2.6. Trunk Model Properties

2.6.1. Principal Component Model

The PC model is based on a set of points associated with the trunk t_P, whose selection was explained in 2.5.4. In addition, the points assumed to be outliers t_O, which surround the trunk, are provided by the model. The three principal components $t_{\overrightarrow{PC_1}}$, $t_{\overrightarrow{PC_2}}$ and $t_{\overrightarrow{PC_3}}$ depend on the inliers t_P only. The $t_{\overrightarrow{PC_1}}$ corresponds to a linear regression model of the trunk, while the residuals $\epsilon(t_P)$ of this regression vector are defined by the PC scores of the second and third component (see Equation (2)).

$$\epsilon(t_P) = \sqrt{\text{scores}(t_P)_2{}^2 + \text{scores}(t_P)_3{}^2} \tag{2}$$

2.6.2. Trunk Orientation

The zenith angle $t_\zeta \in [0, 90[$ (Equation (3)) describes the angle deviation of $t_{\overrightarrow{PC_1}}$ (the trunk) to a vertical line.

$$t_\zeta = \frac{\cos^{-1}\left(t_{\overrightarrow{PC_1}_3}\right)}{\sqrt{t_{\overrightarrow{PC_1}_1}^2 + t_{\overrightarrow{PC_1}_2}^2 + t_{\overrightarrow{PC_1}_3}^2}} \tag{3}$$

The azimuth angle $t_\alpha \in [0, 360[$ (Equation (4)) describes the deviation of $t_{\overrightarrow{PC_1}}$ from the northern direction which indicates the leaning direction of the trunk.

$$t_\alpha = \tan^{-1}\left(\frac{t_{\overrightarrow{PC_1}_1}}{t_{\overrightarrow{PC_1}_2}}\right) \tag{4}$$

2.6.3. Position

The centre point t_c (Equation (5)) of the model corresponds to the spatial centre of the points t_P associated with the trunk which were used to fit the model.

$$t_c = \left(\overline{t_{Px}}, \overline{t_{Py}}, \overline{t_{Pz}}\right) \tag{5}$$

An advantage of the principal component line fitting approach is that the coordinates of every point of the trunk can be calculated as a linear combination of the first principal component $t_{\overrightarrow{PC_1}}$ and the centre point t_c. Therefore a point p_k on this regression line can be calculated by Equation (6), in which the scalar k corresponds to the desired height along the growth direction of the trunk relative to the centre point c_t:

$$p_k = k \cdot t_{\overrightarrow{PC_1}} + t_c \tag{6}$$

This feature is used to estimate the position of the trunk t_p, while the z-component of the t_p coordinate should be zero. Therefore the parameter k is estimated by Equation (7), in which t_ζ corresponds to the zenith angle of the trunk and h to the height of the centre point t_c.

$$k = \frac{h}{\cos(t_\zeta)} \tag{7}$$

The trunk top position t_{top} corresponds to the modelled centre of the trunk at the assumed CBH height. It can be calculated corresponding to the ground position by using Equation (6), while the parameter k is set to the assumed height of the trunk (see Section 2.6.4).

2.6.4. Trunk Height

The height of a trunk t_h is implicitly given by the expected crown base height Z_{CBH} (see Section 2.5.2). The length of a trunk t_l is calculated by Equation (7), in which the variable h is set to Z_{CBH}.

2.6.5. Quality Criteria

The quality of a trunk model is evaluated by different criteria. Apart from the classical MSE, the MEPL (mentioned in 2.5.4) or the uniform distribution criterion (t_{χ^2}) of the points associated with the

trunk can be used. The t_{MSE} is based on the residuals $\epsilon\left(t_P\right)$ of the regression line (Equation (8)), while t_{MEPL} is defined by Equation (9). The uniform distribution criterion of the inliers is calculated by applying a *Chi-Square Test* on the pair-wise distance according to their sorted $t_{\overrightarrow{PC_1}}$ scores.

$$t_{MSE} = \overline{\epsilon(t_P)^2} \tag{8}$$

$$t_{MEPL} := \frac{\max\left(\epsilon(t_P)\right)}{\max(t_{P_z}) - \min(t_{P_z})} \tag{9}$$

2.7. Methods of Evaluation

To carry out an evaluation of the *aTrunk* approach, it was applied to the ALS point cloud of the study area. The measured GNSS positions and derived TLS trunk positions served as reference datasets. To minimise systematic errors both the GNSS and the TLS positions were adjusted to the detected positions using an affine point set registration. A detected trunk position was assumed to correspond to its reference position when its distance was below 4 m. In addition, the selection was limited to the extent of the reference datasets. It should be noted that both reference datasets did not include all trunks because some trees were not measured or not detected by the slicing approach.

A local maxima-based *watershed* segmentation—similar to the approach used by Hyyppä *et al.* [3])—served as benchmark, which identifies the trees using assumed water basins and dams. A raster model with 0.5 m × 0.5 m pixels, using the maximum point elevation for each pixel, was generated and smoothed by a 5 m × 5 m *Gaussian*-filter. The trees were identified by the watershed-segmentation-tool of *SAGA* (*cf.* [39]). For each segment the coordinates of the pixel with maximum value were considered as a tree position when the value was above 15 m.

To get information about the potential accuracy improvement of the *aTrunk* approach to the *watershed* approach, the *matching* positions (distance below 4 m) were identified. A *combined* dataset was generated using both the *aTrunk* and *watershed* positions. In case of corresponding positions the *aTrunk* positions were preferred. An accuracy assessment of the *aTrunk*, *watershed*, *matching* and *combined* positions was performed using the TLS positions as reference. Due to the large location residuals, the GNSS reference dataset was rejected for further evaluation.

A sensitivity analysis of the the *aTrunk* approach was performed in two steps. Firstly the parameters were optimised by applying the algorithm repeatedly to the study area with a large number of randomly selected parameter sets. The TLS positions served as reference to quantify the accuracy, while the positions were assigned automatically (with a maximum distance of 3 m). A parameter combination (illustrated in Table 1) with a high detection rate maintained for the study area. For the second step of the sensitivity analysis, the chosen set served as initial values, while each parameter was varied in its reasonable range of values.

Table 1. Model Parameters

Parameter Name	Values' Range	Unit	Description	Value in This Study	Reference Section
$minPoints$ (n_{min})	$\mathbb{N}_{>1}$	–	Minimum number of points assumed to form a trunk	4	2.5.4
$maxPointsF$ (f_{max})	$\mathbb{R}^+$	–	Adaptive maximum number of points forming a trunk	5.0	2.5.4
$overlap$	$\mathbb{R}_0^+$	m	Width of the overlapping area	5	2.5.1
$maxSampleSize$	$\mathbb{R}^+$	m	Maximum xy-size of a sample before trunk identification	5	2.5.1
$hwRel$	$\mathbb{R}^+$	–	Minimum ratio between z- and xy-range of a trunk	3.0/1.0	2.5.4
$minZRange$	$\mathbb{R}_0^+$	m	Minimum height of a trunk	3.0	2.5.4
$groundCoverLevel$ (Z_{GCV})	$\mathbb{R}$	m	Maximum height of ground-covering vegetation	1.0	2.5.2
$minCBH$ (ρ_{min})	$[0,1]$	–	Assumed minimum relative crown base height	0.35	2.5.2
$maxCBH$ (ρ_{max})	$[\rho_{min},1]$	–	Assumed maximum relative crown base height	0.65	2.5.2
$defaultCBH$ (ρ_d)	$[\rho_{min},\rho_{max}]$	–	Default relative crown base height	0.45	2.5.2
$thCBH$	$\mathbb{R}^+$	–	Threshold for crown base height estimation	0.3	2.5.2
$delta$ (δ)	$\mathbb{R}^+$	m	Maximum distance of clustering algorithm.	1.5	2.5.3
$cMinPts$	$\mathbb{N}$	-	Minimum neighbours of a point in a cluster	2	2.5.3
$zBufferScale$	$\mathbb{R}_0^+$	–	Scale factor of z-axis for 3D clustering	0.1	2.5.3
$MEPL$	$\mathbb{R}_0^+$	m	Expected maximum error per length of trunk	0.07	2.5.4
$maxZenith$	$[0,90[$	°	Maximum assumed zenith angle of a trunk	10	2.5.4
$relOutliers$	$[0,1[$	–	Expected maximum ratio of t_P and t_O vs. t_O	0.7	2.5.4
$uniformProb$ (χ^2)	$[0,1]$	–	Assumed minimum unique distribution of the z-values	0.001	2.6.5
$mergeBuffer$	$\mathbb{R}_0^+$	m	Assumed minimum distance between two trunks	1.8	2.5.5

3. Results and Discussion

3.1. Sensitivity Analysis

For the evaluation of the results of the sensitivity analysis, the parameters were grouped by their qualitative effect on the results (see Table 2). Selected parameters are illustrated in Figures 6–8 while other parameters can be found in the supplement.
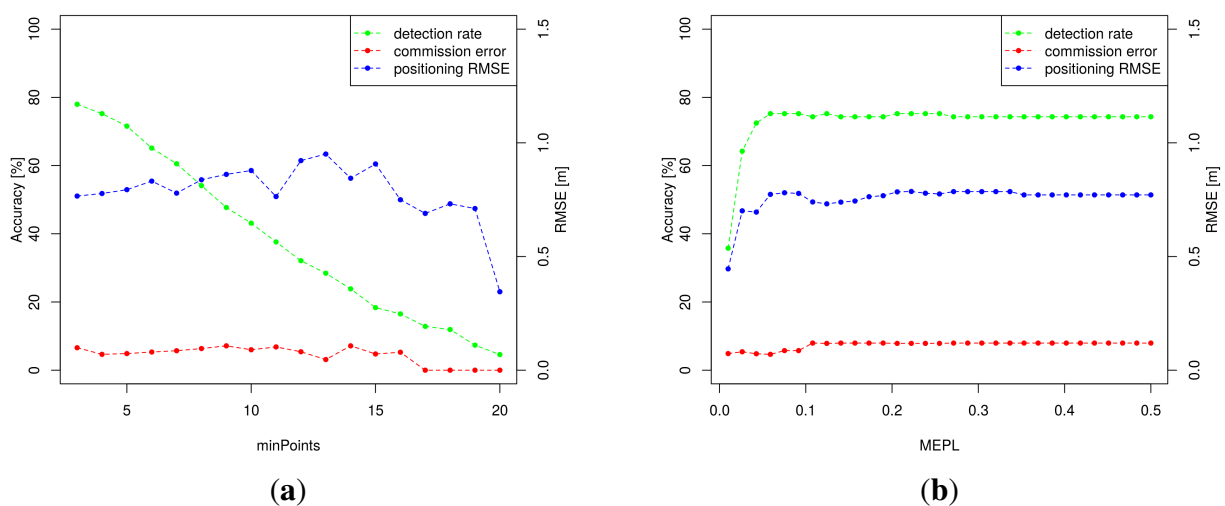

(a)   **(b)**

Figure 6. Sensitivity analysis of selected parameters controlling the model quality (Group 2). (**a**) Minimum number of points n_{min}; (**b**) Quality criterion $MEPL$.
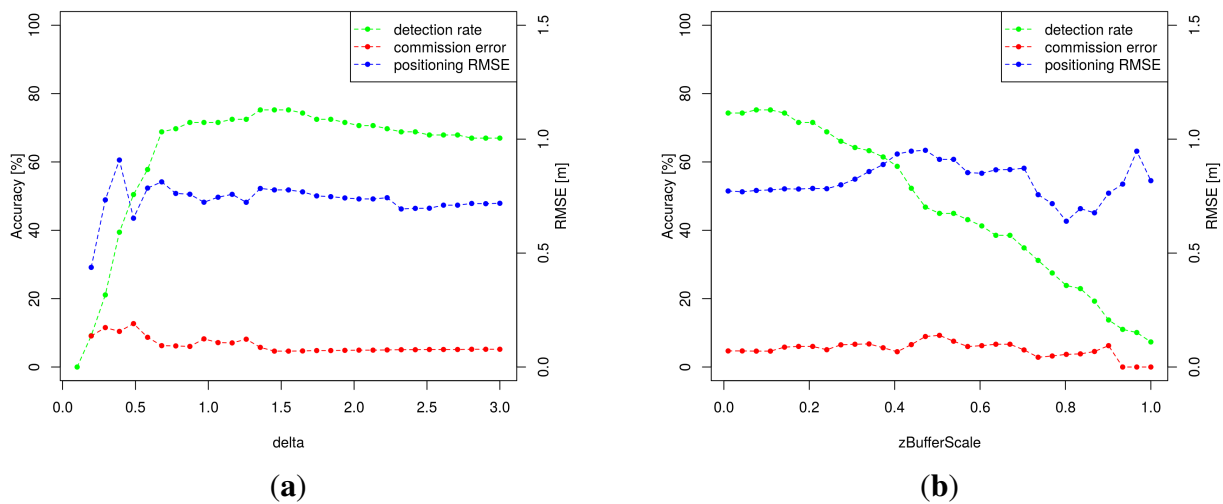
Figure 7. Sensitivity analysis of selected parameters controlling the clustering (Group 4). (**a**) Cluster parameter δ; (**b**) Cluster parameter $zBufferScale$.
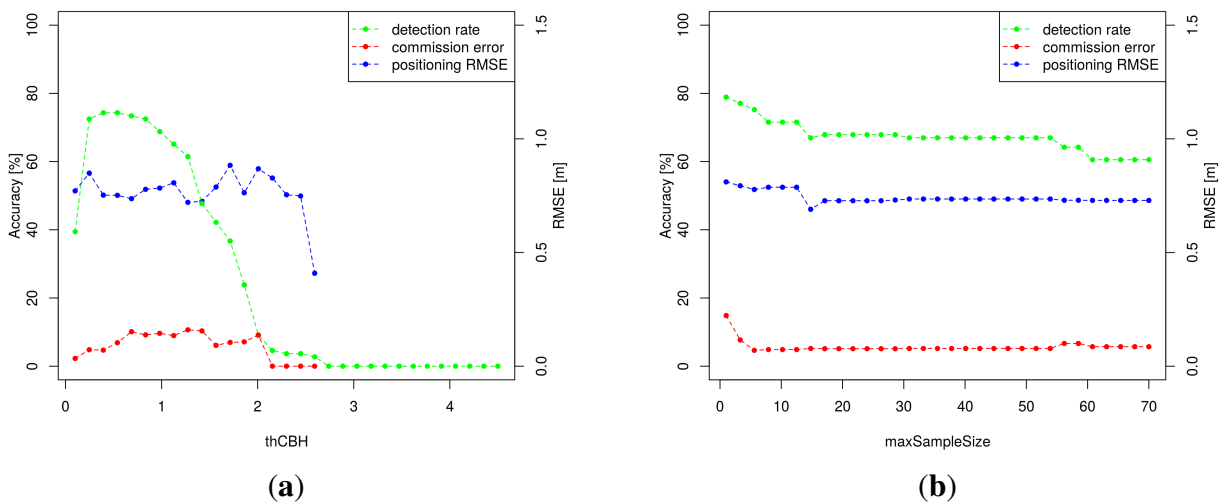

Figure 8. Sensitivity analysis of selected parameters controlling the CBH estimation (Group 5). (**a**) Crown base height threshold $thCBH$, with $\rho_d = 0$; (**b**) Sample size parameter $maxSampleSize$.

Table 2. Parameter Groups

Group	Parameters	Expected Effect on Results
1	$overlap, f_{max}, hwRel, relOutliers$	Control the computation effort
2	$n_{min}, MEPL, \chi^2, maxZenith$	Control the trunk model accuracy
3	$mergeBuffer, \rho_{min}, \rho_{max}, \rho_d, Z_{GCV}, minZRange$	Rely on stand structure
4	$\delta, zBufferScale, cMinPts$	Control the clustering
5	$maxSampleSize, thCBH$	Control the CBH estimation

Group 1: *Group 1* controls the computation effort and has—in a reasonable range of values—a low influence on the accuracy. The parameter $overlap$ should be larger than the assumed average tree distance to ensure identifying all points of a trunk.

Group 2: *Group 2* defines the demands of the user to the trunk model accuracy while stricter demands result in reduced commission errors or improved positioning accuracies but also in reduced detection rates. Figure 6a illustrates that the detection rate decreases the higher n_{min} is chosen. Although the effect of n_{min} on the commission errors is low for the study area, a positive effect is expected for more dense point clouds and larger n_{min} values. The parameter $MEPL$ (Figure 6b) leads to reduced commission errors for values below 0.1 m while the detection rate decreases clearly for values below 0.05 m caused by an overestimation of the number of outliers. The parameter $maxZenith$ ensures finding almost vertical trunk models which results in a slightly optimised RMSE. A value above $5°$ is recommended to reduce omissions. The parameter χ^2, which ensures a certain uniform distribution of the point in growing direction, has shown to be unsuitable to reduce the commission errors.

Group 3: The values of *Group 3* conform to forest characteristics, which are not known exactly a priori. Nevertheless the parameter $mergeBuffer$ is widely stable for about the assumed minimum distance between two trunks. The parameters ρ_{min}, ρ_{max} and ρ_d—which support the automated CBH estimation—are estimated by expert knowledge. Assuming a correct automated CBH estimation, these parameters should have no influence on the results. The parameter Z_{GCV} reduces the detection rate for higher values, because the number of available points in the lower trunk section is decreased. For the study area the minimum trunk height $minZRange$ has a low influence on the commission error, while values above 5 m reduce the detection rate. Nevertheless it is assumed that for vertically inhomogeneous forest stands stricter demands on $minZRange$ will minimise the commission errors.

Group 4: The parameters of *Group 4* are necessary due to the clustering concept and are affected by the point density, vertical point distribution and noise. It is recommended to optimise the parameters δ (Figure 7a), $zBufferScale$ (Figure 7b) and $cMinPts$ for each dataset.

Group 5: *Group 5* controls the CBH estimation accuracy. The parameter $maxSampleSize$ (Figure 8b) ensures a local estimation of the CBH, which results in an increased detection rate for small values, but also in increased commission errors. These incorrect detections are caused by trees, which are divided into small point groups. Such points are identified as a trunk, because the low horizontal extent results in a vertical arrangement similar to a trunk. A $maxSampleSize$ value of about the average crown diameter is proposed. The threshold value $thCBH$ has a great impact on the detection rate (Figure 8a), because for values chosen too large the trunk models reach into the crown and for small values the available number of points is reduced, which both result in inaccurate trunk models and omissions. For the analysis of $thCBH$ the parameter ρ_d was set to zero, because the threshold range defined by ρ_{min} and ρ_{max} as well as ρ_d conceal wrong CBH estimations.

3.2. Evaluation

Table 3 illustrates the accuracy assessment using the TLS-derived trunk positions as reference. The assignment of the detected positions to the reference positions is visualised in Figure 9. The detection rate, precision and overall accuracy is calculated according to Yu *et al.* [13].

Table 3. Accuracy assessment of the different approaches.

Approach	Detection Rate	Precision	Overall Accuracy	Position Error	
				Average	**RMSE**
watershed	91%	85%	88%	1.04 m	1.25 m
aTrunk	75%	95%	84%	0.59 m	0.78 m
matching	69%	96%	80%	0.64 m	0.82 m
combined	98%	86%	92%	0.67 m	0.85 m
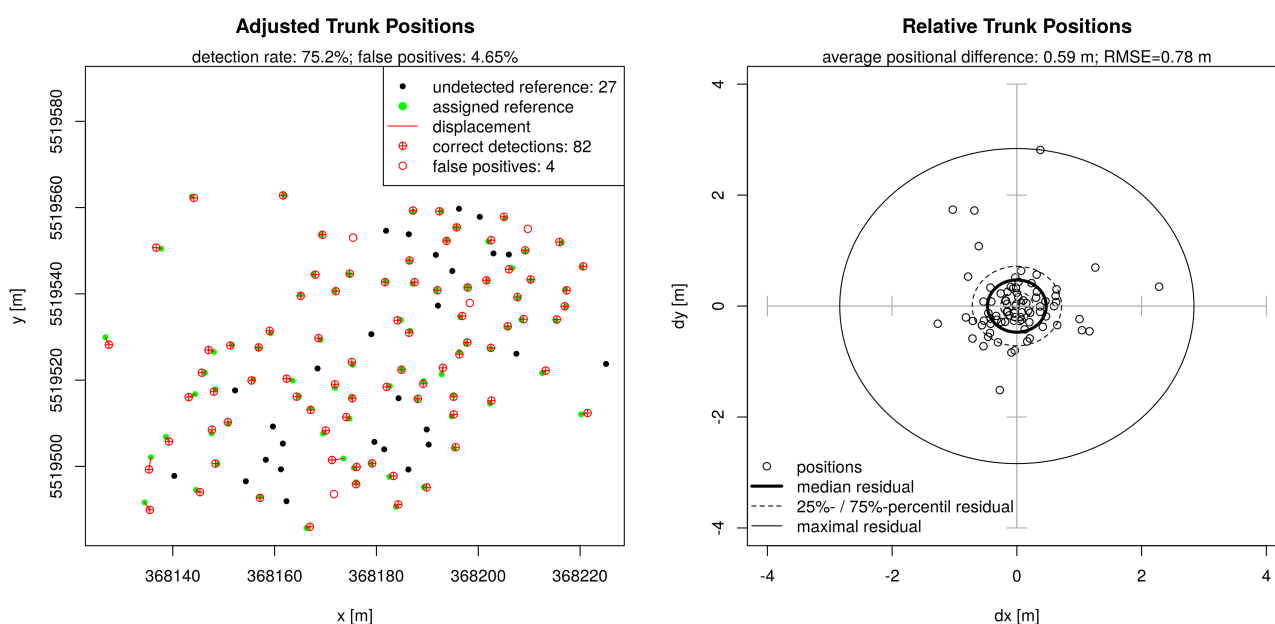
Figure 9. Evaluation of the detected *aTrunk* positions using the TLS positions as reference. The left image illustrates the assignment of the positions using absolute coordinates. The right image illustrates the relative positional differences between the reference positions and the corresponding detected positions.

The detection rate of the *aTrunk* approach is clearly outnumbered by the detection rate of the *watershed* approach. This is mainly due to the effect that not all trunks are recorded by the ALS data. In addition the homogeneous stand structure benefits the crown identification. The precision of the *aTrunk* approach is clearly better compared to the *watershed* results, because the point structure of trunks is less ambiguous compared to crown shapes which are partially merged. Nevertheless, other crown segmentation approaches could reach better results for this dataset.

The actual benefit of a trunk detection compared to a crown detection is the high accuracy in positioning, which significantly increases the positioning accuracy of the *combined* approach compared to the *watershed* approach. The improvement of the mean positioning error of about 32% supports the results of Reitberger *et al.* [12] which mention an improvement of up to 25%. The remaining residuals are mainly caused by branches and the trunk diameter. In addition uncertainties of the ALS positions (horizontal accuracy of about 5 to 15 cm assumed by May and Toth [40]) and of the TLS reference

positions are remaining. Nevertheless the inaccurate GNSS measurements imply that the trunk detection can be superior to ground-based GNSS positioning.

As the trunk detection is independent from the crown detection, the *matching* positions can be used as particularly reliable tree positions. The remaining commission error is partially caused by incomplete reference positions because of covered trees in the TLS data.

3.3. Modelling Results

Figures 10 and 11 illustrate the modelling results of the study area and the larger $1\,\text{km}^2$ sample using the same parametrisation. The homogeneously tall trees of the study area result in long detected trunks, with a mean value of $16.5\,\text{m}$ and a standard deviation (SD) of $2.5\,\text{m}$. In comparison, the $1\,\text{km}^2$ sample consists of different areas with varying tree heights. This results in a high standard deviation of about $2.7\,\text{m}$. The MSE distribution of the points associated with the trunk is right-skewed for both datasets. A median of $0.15\,\text{m}$ is reached for the study area and of about $0.06\,\text{m}$ for the $1\,\text{km}^2$ sample.
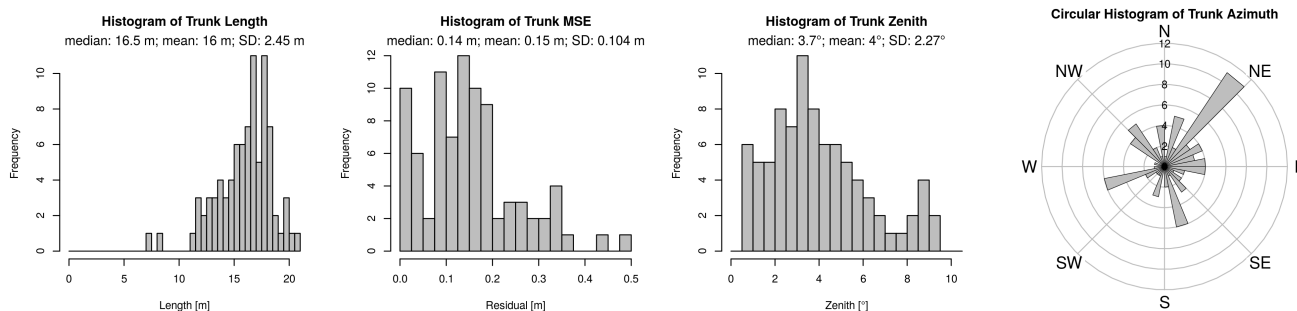

Figure 10. Modelling results of the study area (86 detected trunks).
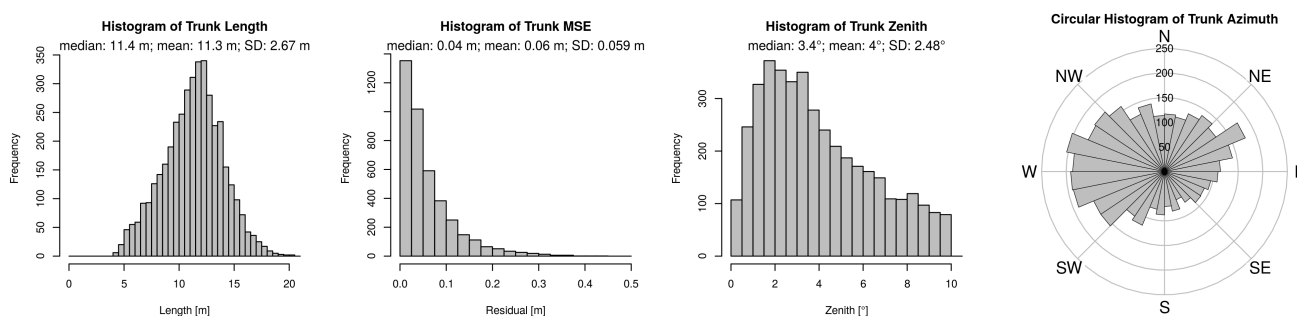

Figure 11. Modelling results of the $1\,\text{km}^2$ sample (4078 detected trunks).

The *zenith* is right-skewed distributed with a median of about $3.5°$, while most of the trunks clearly differ from a vertical orientation. The circular histogram of the trunk azimuth implies a preferred east-west or west-east orientation of the trunks. Under the assumption of low systematic measurement errors, this effect could be caused by the stand characteristics (e.g., soil conditions, topography or dominant wind direction).

3.4. Model Performance

The objective of this paper was the development of a rapid algorithm which is capable of detecting single tree trunks independent from a crown identification. It has been shown that the number of false detections of the *aTrunk* approach is low. On a *Dell Precision T1500* with an *Intel Core i5-750* processor and 8 GB RAM, the algorithm reached a computation time of about 13 s (0.2 s data loading and 12.7 s analysis) for the study area and about 7 min (13 s data loading and 461 s analysis) for the larger $1\,km^2$ sample.

A sensitivity analysis of the effects of data quality (e.g., point density, recording angle), stand structure (e.g., tree species, suppressed trees, inhomogeneous vertical structure, tree number, canopy density), seasonal conditions and terrain (e.g., morphology, steep or varying terrain) has to be performed in a further study including an evaluation of the orientation information, to provide a tool which is capable of supporting operational forest surveys. The additional information about the trunk orientation could help to improve the characterisation of forest stands.

3.5. Model Concept

The presented approach is related to the trunk detection module of Reitberger *et al.* [12], so the overall concepts—ground covering vegetation cut-off, CBH estimation, clustering and line fitting—were adopted. The *RANSAC* concept has been replaced by a deterministic modification of *LO-RANSAC* using a length-dependent quality criterion, and the 2D hierarchical clustering has been replaced by a 3D variation of *DBSCAN*. Especially, the non-overlapping crown segmentation has been exchanged with partially overlapping rectangular segments allowing a seamless tree trunk detection and a multi-core computation.

Current drawbacks are caused by the simplified CBH estimation, insufficient rules to decide if a point group represents a trunk, the simplified removal of ground covering vegetation, and not explicitly considering the characteristics of dominated trees. The CBH estimation could be optimised by more advanced methods (e.g., [41,42]). The sampling technique with overlapping areas leads to an additional computation effort. An alternative method which joins the points associated with trunks to a single dataset may reduce the computation effort under the assumption that the clustering can be done efficiently. Visual inspections had shown that trees which slightly cross the border of a segment can result in incorrect detections, because the isolated points may be aligned in a line. The rules which are used to decide if a point group represents a trunk need to be evaluated and refined to get optimal results.

Independently from the performed sensitivity analysis, the modelling concept implies that the approach depends on a high point density in the trunk section and clearly separable trunks, caused by the assumption of a linear arrangement of points associated with the trunks. So the approach is limited to forest stands with spatially distinguishable trunks where the canopy is permeable for the ALS beams. In addition low-branched trunks (like beech compared to spruce) and leaf off conditions are preferred, while a higher point density could optimise the trunk detection accuracy.

4. Conclusions

This paper presented a trunk detection approach which is independent from a crown identification and works seamlessly on the entire observation area avoiding non-overlapping segments. It derives reliable models (below 5% commission error), which are accurate in positioning (0.78 m RMSE). The models provide—next to the position—information about the trunk length, trunk orientation and point distribution (e.g., in growing direction). With a general focus on the computation effort, the algorithm is designed to be a potential tool for supporting operational forest surveys.

It has also been confirmed that the combination of the trunk positions with a crown-based tree detection is suitable to significantly improve the accuracy in tree positioning (32% for the study site). The independent detections result in a mutual confirmation of the tree positions which leads to decreased commission errors. In addition a preferred leaning direction of trunks was observed, which should be evaluated in further studies.

The algorithm has to be further evaluated regarding data quality, stand structure, seasonal conditions and terrain. It should also be evaluated whether the trunk detection is suitable to reduce the dependency of the tree size on the accuracy of detected tree locations which results in more accurate positions for taller trees [11].

Author Contributions

Sebastian Lamprecht as the main author developed and implemented the approach, led the data acquisition, analysed the data and is responsible for the content of the manuscript. Sandra Dotzler, Erik Haß and Johannes Stoffels took part in the validation data acquisition. Thomas Udelhoven and Johannes Stoffels initiated the study and cross-checked the manuscript.

Conflicts of Interest

The authors declare no conflict of interest.

References

1. Maes, W.H.; Fontaine, M.; Rongé, K.; Hermy, M.; Muys, B. A quantitative indicator framework for stand level evaluation and monitoring of environmentally sustainable forest management. *Ecol. Indic.* **2011**, *11*, 468–479.
2. Strîmbu, V.F.; Strîmbu, B.M. A graph-based segmentation algorithm for tree crown extraction using airborne LiDAR data. *ISPRS J. Photogramm. Remote Sens.* **2015**, *104*, 30–43.

3. Hyyppä, J.; Yu, X.; Hyyppä, H.; Vastaranta, M.; Holopainen, M.; Kukko, A.; Kaartinen, H.; Jaakkola, A.; Vaaja, M.; Koskinen, J.; *et al.* Advances in forest inventory using airborne laser scanning. *Remote Sens.* **2012**, *4*, 1190–1207.

4. Lafond, V.; Lagarrigues, G.; Cordonnier, T.; Courbaud, B. Uneven-aged management options to promote forest resilience for climate change adaptation: effects of group selection and harvesting intensity. *Ann. For. Sci.* **2013**, *71*, 173–186.

5. Kania, A.; Lindberg, E.; Schroiff, A.; Mücke, W.; Holmgren, J.; Pfeifer, N. Individual tree detection as input information for Natura 2000 habitat quality mapping. In Proceedings of the Remote Sensing and GIS for Monitoring Habitat Quality—RSGIS4HQ, Vienna, Austria, 24–25 September 2014.

6. Holmgren, J.; Persson, A.; Söderman, U. Species identification of individual treesHolmgren by combining high resolution LiDAR data with multi-spectral images. *Int. J. Remote Sens.* **2008**, *29*, 1537–1552.

7. Ørka, H.O.; N\a esset, E.; Bollandsås, O.M. Classifying species of individual trees by intensity and structure features derived from airborne laser scanner data. *Remote Sens. Environ.* **2009**, *113*, 1163–1174.

8. Yu, X.; Litkey, P.; Hyyppä, J.; Holopainen, M.; Vastaranta, M. Assessment of low density full-waveform airborne laser scanning for individual tree detection and tree species classification. *Forests* **2014**, *5*, 1011–1031.

9. Jakubowski, M.K.; Li, W.; Guo, Q.; Kelly, M. Delineating individual trees from LiDAR data: A comparison of vector-and raster-based segmentation approaches. *Remote Sens.* **2013**, *5*, 4163–4186.

10. Leiterer, R.; Mücke, W.; Hollaus, M.; Pfeifer, N.; Schaepman, M.E. Operational forest structure monitoring using airborne laser scanning. *Photogramm. Fernerkund. Geoinf.* **2013**, *2013*, 173–184.

11. Kaartinen, H.; Hyyppä, J.; Yu, X.; Vastaranta, M.; Hyyppä, H.; Kukko, A.; Holopainen, M.; Heipke, C.; Hirschmugl, M.; Morsdorf, F.; *et al.* An international comparison of individual tree detection and extraction using airborne laser scanning. *Remote Sens.* **2012**, *4*, 950–974.

12. Reitberger, J.; Schnörr, C.; Krzystek, P.; Stilla, U. 3D segmentation of single trees exploiting full waveform LIDAR data. *ISPRS J. Photogramm. Remote Sens.* **2009**, *64*, 561–574.

13. Yu, X.; Litkey, P.; Hyyppä, J.; Holopainen, M.; Vastaranta, M. Assessment of low density full-waveform airborne laser scanning for individual tree detection and tree species classification. *Forests* **2014**, *5*, 1011–1031.

14. Chen, Q.; Baldocchi, D.; Gong, P.; Kelly, M. Isolating individual trees in a savanna woodland using small footprint LiDAR data. *Photogramm. Eng. Remote Sens.* **2006**, *72*, 923–932.

15. Koch, B.; Heyder, U.; Weinacker, H. Detection of individual tree crowns in airborne LiDAR data. *Photogramm. Eng. Remote Sens.* **2006**, *72*, 357–363.

16. Zhou, J.; Proisy, C.; Descombes, X.; Hedhli, I.; Barbier, N.; Zerubia, J.; Gastellu-Etchegorry, J.P.; Couteron, P. Tree Crown Detection in High Resolution Optical and LiDAR Images of Tropical Forest. Available online: http://citeseerx.ist.psu.edu/viewdoc/download? doi=10.1.1.393.1014& rep=rep1&type=pdf (accessed on 16 April 2015).

17. Duncanson, L.I.; Cook, B.D.; Hurtt, G.C.; Dubayah, R.O. An efficient, multi-layered crown delineation algorithm for mapping individual tree structure across multiple ecosystems. *Remote Sens. Environ.* **2014**, *154*, 378–386.

18. Wang, Y.; Weinacker, H.; Koch, B. A LiDAR point cloud based procedure for vertical canopy structure analysis and 3D single tree modelling in forest. *Sensors* **2008**, *8*, 3938–3951.

19. Morsdorf, F.; Meier, E.; Kötz, B.; Itten, K.I.; Dobbertin, M.; Allgöwer, B. LiDAR-based geometric reconstruction of boreal type forest stands at single tree level for forest and wildland fire management. *Remote Sens. Environ.* **2004**, *92*, 353–362.

20. Gupta, S.; Koch, B.; Weinacker, H. Tree Species Detection Using Full Waveform LiDAR Data in a Complex Forest. Available online: http://www.isprs.org/proceedings/xxxviii/part7/b/pdf/249_XXXVIII-part7B.pdf (accessed on 17 April 2015).

21. Lindberg, E.; Holmgren, J.; Olofsson, K.; Wallerman, J.; Olsson, H. Estimation of tree lists from airborne laser scanning using tree model clustering and k-MSN imputation. *Remote Sens.* **2013**, *5*, 1932–1955.

22. Lee, H.; Slatton, K.C.; Roth, B.E.; JR, W.P.C. Adaptive clustering of airborne LiDAR data to segment individual tree crowns in managed pine forests. *Int. J. Remote Sens.* **2010**, *31*, 117–139.

23. Leiterer, R.; Morsdorf, F.; Torabzadeh, H.; Schaepman, M.; Mucke, W.; Pfeifer, N.; Hollaus, M. A voxel-based approach for canopy structure characterization using full-waveform airborne laser scanning. In Proceedings of the 2012 IEEE International Geoscience and Remote Sensing Symposium (IGARSS), Munich, Germany, 22–27 July 2012; pp. 3399–3402.

24. Eysn, L.; Hollaus, M.; Lindberg, E.; Berger, F.; Monnet, J.M.; Dalponte, M.; Kobal, M.; Pellegrini, M.; Lingua, E.; Mongus, D.; *et al*. A benchmark of LiDAR-based single tree detection methods using heterogeneous forest data from the Alpine space. *Forests* **2015**, *6*, 1721–1747.

25. Vincent, L.; Soille, P. Watersheds in digital spaces: An efficient algorithm based on immersion simulations. *IEEE Trans. Pattern Anal. Mach. Intell.* **1991**, *13*, 583–598.

26. Fischler, M.A.; Bolles, R.C. Random sample consensus: A paradigm for model fitting with applications to image analysis and automated cartography. *Commun. ACM* **1981**, *24*, 381–395.

27. Abd Rahman, M.; Gorte, B.; Bucksch, A. A new method for individual tree delineation and undergrowth removal from high resolution airborne lidar. In Proceedings of the ISPRS Workshop Laserscanning 2009, Paris, France, 1–2 September 2009.

28. Lu, X.; Guo, Q.; Li, W.; Flanagan, J. A bottom-up approach to segment individual deciduous trees using leaf-off LiDAR point cloud data. *ISPRS J. Photogramm. Remote Sens.* **2014**, *94*, 1–12.

29. Edson, C.; Wing, M.G. Airborne light detection and ranging (LiDAR) for individual tree stem location, height, and biomass measurements. *Remote Sens.* **2011**, *3*, 2494–2528.

30. Landesamt für Vermessung und Geobasisinformation Rheinland-Pfalz (LVermGeo). Luftbild RP Basisdienst. Available online: http://www.geoportal.rlp.de/mapbender/php/wms.php?layer_id=30692&PHPSESSID=02dbaf5a20e411b1c46de1f8ef2a9cdd&REQUEST=GetCapabilities&VERSION=1.1.1&SERVICE=WMS (accessed on 25 September 2014).

31. Topcon Corporation. HiPer V—Dual-Frequency GNSS Receiver. Available online: http://www.topconpositioning.com/sites/default/files/HiPer_V_Broch_7010_2121_RevB_TF_sm.pdf (accessed on 8 Dezember 2014).

32. FARO Europe GmbH. FARO® Laser Scanner Photon 120/20. Available online: http://www.faroeurope.com/portal/htdocs/download.php?id=1794&type=DOC&SiteCatalyst=true (accessed on 13 September 2014).

33. Bienert, A.; Maas, H.G.; Scheller, S. Analysis of the information content of terrestrial laserscanner point clouds for the automatic determination of forest inventory parameters. In Proceedings of the Workshop on 3D Remote Sensing in Forestry, Vienna, Austria, 14–15 February 2006.

34. EDF R&D. CloudCompare – 3D Point Cloud and Mesh Processing Software Open Source Project. Available online: http://www.cloudcompare.org/ (accessed on 14 November 2014).

35. Python Software Foundation. python. Available online: https://www.python.org (accessed on 9 February 2015).

36. Ester, M.; Kriegel, H.P.; Sander, J.; Xu, X. A Density-Based Algorithm for Discovering Clusters in Large Spatial Databases with Noise. Available online: https://www.aaai.org/Papers/KDD/1996/KDD96-037.pdf (accessed on 17 April 2015).

37. Wold, S.; Esbensen, K.; Geladi, P. Principal component analysis. *Chemom. Intell. Lab. Syst.* **1987**, *2*, 37–52.

38. Chum, O.; Matas, J.; Kittler, J. Locally optimized RANSAC. In *Pattern Recognition*; Michaelis, B., Krell, G., Eds.; Springer: Berlin/Heidelberg, Germany, 2003; pp. 236–243.

39. SAGA User Group Association. System for Automated Geoscientific Analyses. Available online: http://www.saga-gis.org/en/index.html (accessed on 28 May 2015).

40. May, N.C.; Toth, C.K. Point positioning accuracy of airborne LiDAR systems: A rigorous analysis. *Int. Arch. Photogramm. Remote Sens. Spat. Inf. Sci.* **2007**, *36*, 107–111.

41. Popescu, S.C.; Zhao, K. A voxel-based LiDAR method for estimating crown base height for deciduous and pine trees. *Remote Sens. Environ.* **2008**, *112*, 767–781.

42. Vauhkonen, J. Estimating crown base height for Scots pine by means of the 3D geometry of airborne laser scanning data. *Int. J. Remote Sens.* **2010**, *31*, 1213–1226.